DELPHI Collaboration DELPHI 2004-020 CONF 695
21 July 2004

Study of Trilinear Gauge Boson Couplings ZZZ, $ZZ\gamma$ and $Z\gamma\gamma$ at LEP

PRELIMINARY

E. Graziani
INFN - Roma Tre
C. Matteuzzi
Università di Milano and INFN
L. Pieri
Università di Roma Tre, and INFN[1]
R.L. Sekulin
Rutherford Appleton Laboratory
V. Verzi
Università di Roma II and INFN
O. Yushchenko
IHEP, Serpukov

Abstract

Trilinear neutral gauge boson couplings ZZZ, $ZZ\gamma$ and $Z\gamma\gamma$ have been studied with the DELPHI detector using data at energies between 183 and 208 GeV. Limits are derived on these couplings from an analysis of the reactions $e^+e^-\to Z\gamma$, using data from the final states $\gamma f\bar{f}$, with $f = q$ or ν, from $e^+e^-\to ZZ$, using data from the four-fermion final states $q\bar{q}q\bar{q}$, $q\bar{q}\mu^+\mu^-$, $q\bar{q}e^+e^-$, $q\bar{q}\nu\bar{\nu}$, $\mu^+\mu^-\nu\bar{\nu}$ and $e^+e^-\nu\bar{\nu}$, and from $e^+e^-\to Z\gamma^*$, in which the final state γ is off mass-shell, using data from the four-fermion final states $q\bar{q}e^+e^-$ and $q\bar{q}\mu^+\mu^-$. No evidence for the presence of such couplings is observed, in conformity with the expectations of the Standard Model.

Contributed Paper for ICHEP 2004 (Beijing)

[1]Now at Università di Torino

1 Introduction

One of the important predictions of the Standard Model which can be tested at LEP2 is its non-Abelian character, leading to the prediction of triple gauge boson couplings. However, while non-zero values of these couplings are predicted for the charged ($WW\gamma$, WWZ) sector, the $SU(2) \times U(1)$ symmetry of the Standard Model predicts the absence of such couplings in the neutral sector, namely at the ZZZ, $ZZ\gamma$ and $Z\gamma\gamma$ vertices. This paper describes an investigation of this prediction by DELPHI using LEP2 data taken between 1997 and 2000 at energies between 183 and 208 GeV.

1.1 Phenomenology of the neutral triple gauge boson vertex

Within the Standard Model, production of two neutral gauge bosons in e^+e^- collisions proceeds at lwest order via the t- or u-channel exchange of an electron. These processes are shown in figure 1, where both on- and off-shell γ production is implied, as is the subsequent decay of the final state Z or off-shell γ into a fermion-antifermion pair. The same figure shows contributions to these reactions which could come from physics beyond the Standard Model via the s-channel exchange of a virtual γ or Z, leading to $Z\gamma$, $Z\gamma^*$ or ZZ production via a neutral triple vector boson coupling.

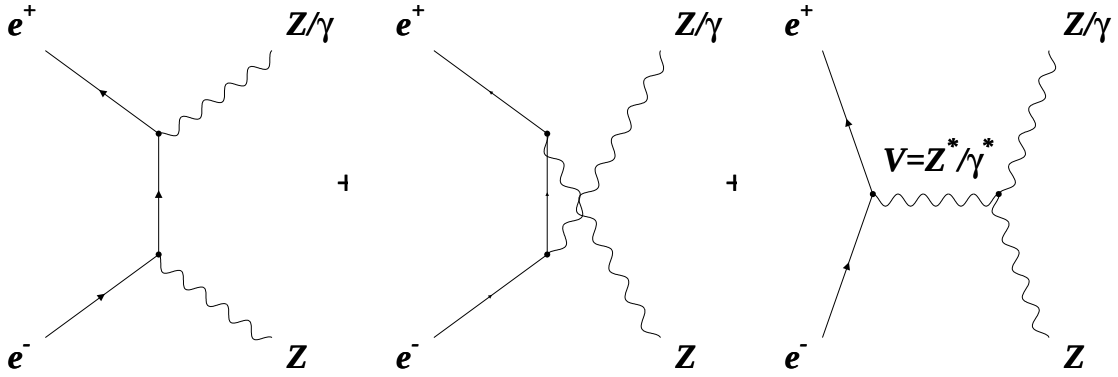

Figure 1: Lowest order Feynman diagrams for the production of two gauge bosons ZZ and$Z\gamma$, where both on- and off-shell γ production is implied. The two diagrams on the left represent the Standard Model contribution, while the third one involves an anomalous interaction among three neutral gauge bosons.

The case where two of the three neutral gauge bosons interacting at the $V_1^0V_2^0V_3^0$ vertex are on mass-shell has been studied in [1]. In this case, there are twelve independent anomalous couplings satisfying Lorentz invariance and Bose symmetry. Calling V the exchanged boson ($V = Z, \gamma$), the couplings f_i^V (i =4,5) produce a ZZ final state and h_i^V ($i = 1 \cdots 4$) the $Z\gamma$ final state. The couplings f_5^V, h_3^V and h_4^V are CP-conserving and f_4^V, h_1^V and h_2^V are CP-violating. There are no couplings common to production of both the ZZ and $Z\gamma$ final states.

A complete phenomenological description of the anomalous neutral gauge couplings in the case where one, two or three of the gauge bosons interacting at the $V_1^0V_2^0V_3^0$ vertex may be off mass-shell has been developed in [2]. Following the treatment of the charged triple gauge boson vertex developed, for instance, in [3, 4], all the Lorentz invariant forms which can contribute to the ZZZ, $ZZ\gamma$ and $Z\gamma\gamma$ vertices are listed, imposing Bose symmetry as

appropriate. An effective Lagrangian model is then developed in terms of the operators of lowest dimension which affect only the neutral triple gauge boson vertex and which are required to reconstruct fully all the vertex forms.[2] This leads to a Lagrangian with operators of dimension, d, ranging from $d = 6$ to $d = 12$. Such an expansion is valid in the case where the New Physics energy scale, Λ, represented by the operators is very high, *i.e.* $\Lambda \gg m_Z$, and the relative contribution from an operator of dimension d may be expected to be suppressed by a factor $1/\Lambda^{(d-4)}$. In the analysis we report here, we have considered only the lowest dimension operators contributing to the parameters we have determined. In addition to satisfying Lorentz and Bose symmetry, the operators are required to be $U(1)_{em}$-invariant, and both CP-conserving operators, $\mathcal{O}$, and CP-violating operators, $\tilde{\mathcal{O}}$, are considered:

$$\mathcal{L} = e\Big(\sum_{i,CP+} \ell_i^{V_1^0 V_2^0 V_3^0} \mathcal{O}_i^{V_1^0 V_2^0 V_3^0} + \sum_{i,CP-} \tilde{\ell}_i^{V_1^0 V_2^0 V_3^0} \tilde{\mathcal{O}}_i^{V_1^0 V_2^0 V_3^0}\Big) . \tag{1}$$

Of the operators included in the sum defined above, some affect the V^0ZZ and $V^0Z\gamma^*$ vertices ($V^0 \equiv Z, \gamma$), some the $V^0Z\gamma^*$ vertex only, and some the $V^0Z\gamma^*$ and $V^0Z\gamma$ vertices; none give contributions to all three vertices. In [2] a connection is made between the coefficients ℓ_i and $\tilde{\ell}_i$ of the operators in the effective Lagrangian describing the general $V_1^0V_2^0V_3^0$ vertex and the dimensionless coefficients h and f describing on-shell $Z\gamma$ and ZZ production, respectively: in the on-shell limit, each of the h and f coefficients (which are dimensionless) is related to one operator of lowest dimension, $d = 6$, as $f, h = \ell^{V_1^0 V_2^0 V_3^0} m_Z^2$.

As in the case of the charged triple gauge boson couplings, a further simplification in the possible structure of the effective Lagrangian may be expected by imposition of $SU(2) \times U(1)$ invariance on its form. Such a form is presented in an addendum to [2], and the effective Lagrangian reduces to a sum of two terms, both with dimension $d = 8$, one ($\mathcal{O}_{SU(2)\times U(1)}$) CP-conserving and one ($\tilde{\mathcal{O}}_{SU(2)\times U(1)}$) CP-violating. This simplification leads to constraints between some of the ${\ell_i}^{V_1^0 V_2^0 V_3^0}$ or ${\tilde{\ell}_i}^{V_1^0 V_2^0 V_3^0}$ defined in equation (1):

$${\ell_1}^{ZZZ} \cot\theta_W = {\ell_1}^{ZZ\gamma} = -{\ell_2}^{Z\gamma\gamma} = -{\ell_1}^{Z\gamma\gamma} \tan\theta_W = \frac{v^2}{4}\ell_{SU(2)\times U(1)} , \tag{2}$$

$${\tilde{\ell}_1}^{ZZZ} \cot\theta_W = {\tilde{\ell}_1}^{ZZ\gamma} = -{\tilde{\ell}_3}^{Z\gamma\gamma} = -{\tilde{\ell}_1}^{Z\gamma\gamma} \tan\theta_W = \frac{v^2}{4}\tilde{\ell}_{SU(2)\times U(1)} , \tag{3}$$

where θ_W is the Weinberg angle, v is the vacuum expectation value of the Higgs field and $\ell_{SU(2)\times U(1)}$, $\tilde{\ell}_{SU(2)\times U(1)}$ are the coefficients of the operators $\mathcal{O}_{SU(2)\times U(1)}$ and $\tilde{\mathcal{O}}_{SU(2)\times U(1)}$, respectively. If applied solely to the on-shell channels $Z\gamma$ and ZZ, these conditions become, respectively:

$$f_5^Z \cot\theta_W = h_3^Z = -f_5^\gamma = h_3^\gamma \tan\theta_W = m_Z^2\frac{v^2}{4}\ell_{SU(2)\times U(1)} , \tag{4}$$

$$f_4^Z \cot\theta_W = h_1^Z = -f_4^\gamma = h_1^\gamma \tan\theta_W = m_Z^2\frac{v^2}{4}\tilde{\ell}_{SU(2)\times U(1)} . \tag{5}$$

[2]The $V_1^0V_2^0V_3^0$ vertex functions receive contributions from both transverse and scalar terms, the latter contributing in the case where one off-shell Z decays to a heavy fermion pair through its axial coupling. In the analysis of LEP data only transverse terms need be considered, due to the negligible contribution of $Z \to t\bar{t}$ decays. The contribution of scalar terms is therefore ignored in the following.

The $SU(2) \times U(1)$-conserving Lagrangian considered in [2] is constructed so as to affect only the neutral gauge boson and Higgs sectors, and an alternative form, which would additionally affect off-mass-shell charged gauge boson production, has been proposed in [5]. This leads to a Lagrangian with four possible terms, two CP-conserving ($\mathcal{O}_8^A$, $\mathcal{O}_8^B$) and two CP-violating ($\tilde{\mathcal{O}}_8^A$, $\tilde{\mathcal{O}}_8^B$) and hence to looser constraints between the possible contributing operators: in each of the sets of conditions (2) - (5) listed above, only the first and third of the three equality signs remain, each related to the coefficients $\ell_8^{A,B}$, $\tilde{\ell}_8^{A,B}$ of the relevant Lagrangian operator by appropriate factors of m_Z and v. In both the stronger and weaker of these sets of constraints (which we refer to as the Gounaris-Layssac-Renard and Alcaraz constraints, with respect to the authorship of references [2] and [5]), the gauge invariant operators all now contribute to all three neutral trilinear gauge boson vertices, V^0ZZ, $V^0Z\gamma^*$ and $V^0Z\gamma$.

In order to study the $V_1^0V_2^0V_3^0$ vertex, three physical final states have been defined from the data: $Z\gamma$, $Z\gamma^*$ and ZZ. The first of these is a three-body final state comprising the Z decay products and a detected photon, while the other two are four-fermion final states with, respectively, one or two fermion-antifermion pairs having mass in the Z region. Given the phenomenology summarized above, we have then chosen to determine the following parameters in our study:

- Using data either from the final states ZZ and $Z\gamma^*$ or from final states $Z\gamma^*$ and $Z\gamma$, values are determined for the coefficients of each of the eight $d = 6$ operators which are related in the on-shell limit to one of the h or f coefficients defined in the on-shell formalism of reference [1]. The values of these parameters are quoted in dimensionless form, $\ell^{V_1^0V_2^0V_3^0} m_Z^2$, so as to be directly comparable with published results using data from the on-shell channels.

- The $V^0Z\gamma^*$ vertex is studied on its own by determining the coefficients of the lowest dimension operators which affect solely these vertices. There are two such operators, both of dimension $d = 8$, one CP-conserving and involving s-channel γ exchange in the production process, and the other CP-violating and involving s-channel Z exchange. Data from the $Z\gamma^*$ and ZZ final states were used in the determination of the coefficients of these operators; it should be noted that the two operators in question affect the whole of the four-fermion phase space, due to the coupling of the off-shell γ to the $f\bar{f}$ system. The coefficients of these operators are, again, quoted in dimensionless form: $\ell^{V_1^0V_2^0V_3^0} m_Z^4$.

- The coefficients of the $SU(2) \times U(1)$-conserving operators are determined, using both the Gounaris-Layssac-Renard and the Alcaraz constraints. They are quoted in a dimensionless form, such that in the on-shell limit they become equal to one of the h_i^V occurring in the constraint equations 4 and 5 above.

A list of the parameters we have determined, the definitions of the operators to which they refer and (where relevant) the on-shell coefficients to which they are related is given in table 1.

1.2 Experimental considerations

Of the three final state channels, $Z\gamma$, ZZ and $Z\gamma^*$, defined in the previous section, the most precise limits on anomalous couplings are derived from the first, when the final

Vertices affected	Parameter	Lagrangian Operator	Related on-shell coefficient
a)			
ZZZ	$\ell_1^{ZZZ} m_Z^2$	$-Z_\sigma(\partial^\sigma Z_\nu)(\partial_\mu Z^{\mu\nu})$	f_4^Z
	$\ell_1^{ZZZ} m_Z^2$	$\tilde{Z}_{\mu\nu}(\partial_\sigma Z^{\sigma\mu})Z^\nu$	f_5^Z
$ZZ\gamma$	$\tilde{\ell}_3^{ZZ\gamma} m_Z^2$	$-(\partial_\mu F^{\mu\beta})Z_\alpha(\partial^\alpha Z_\beta)$	f_4^γ
	$\ell_2^{ZZ\gamma} m_Z^2$	$\tilde{Z}^{\mu\nu} Z_\nu(\partial^\sigma F_{\sigma\mu})$	f_5^γ
	$\tilde{\ell}_1^{ZZ\gamma} m_Z^2$	$-F^{\mu\beta} Z_\beta(\partial^\sigma Z_{\sigma\mu})$	h_1^Z
	$\ell_1^{ZZ\gamma} m_Z^2$	$-\tilde{F}_{\mu\nu} Z^\nu(\partial_\sigma Z^{\sigma\mu})$	h_3^Z
$Z\gamma\gamma$	$\tilde{\ell}_1^{Z\gamma\gamma} m_Z^2$	$-(\partial^\sigma F_{\sigma\mu})Z_\beta F^{\mu\beta}$	h_1^γ
	$\ell_1^{Z\gamma\gamma} m_Z^2$	$-\tilde{F}_{\rho\alpha}(\partial_\sigma F^{\sigma\rho})Z^\alpha$	h_3^γ
b)			
$ZZ\gamma$	$\tilde{\ell}_4^{ZZ\gamma} m_Z^4$	$\partial^\mu F_{\mu\nu}(\Box\partial^\nu Z_\alpha)Z^\alpha$	–
$Z\gamma\gamma$	$\ell_2^{Z\gamma\gamma} m_Z^4$	$\Box\tilde{F}^{\mu\nu}(\partial^\sigma F_{\sigma\mu})Z_\nu$	–
c) i)			
ZZZ $ZZ\gamma$ $Z\gamma\gamma$	$-\cot\theta_W m_Z^2 \frac{v^2}{4}\tilde{\ell}_{SU(2)\times U(1)}$	$iB_{\mu\nu}(\partial_\sigma B^{\sigma\mu})(\Phi^\dagger D^\nu\Phi)$	h_1^γ
	$-\cot\theta_W m_Z^2 \frac{v^2}{4}\ell_{SU(2)\times U(1)}$	$i\tilde{B}_{\mu\nu}(\partial_\sigma B^{\sigma\mu})(\Phi^\dagger D^\nu\Phi)$	h_3^γ
ii)			
$ZZ\gamma$	$-\cot\theta_W m_Z^2 \frac{v^2}{4}\tilde{\ell}_8^A$	$iB_{\mu\nu}(\partial_\sigma B^{\sigma\mu})(\Phi^\dagger D^\nu\Phi)$	h_1^γ
	$-\cot\theta_W m_Z^2 \frac{v^2}{4}\ell_8^A$	$i\tilde{B}_{\mu\nu}(\partial_\sigma B^{\sigma\mu})(\Phi^\dagger D^\nu\Phi)$	h_3^γ
ZZZ $Z\gamma\gamma$	$-\cot\theta_W m_Z^2 \frac{v^2}{4}\tilde{\ell}_8^B$	$iB_{\mu\nu}(\partial_\sigma W_I^{\sigma\mu})(\Phi^\dagger\tau_I D^\nu\Phi)$	h_1^Z
	$-\cot\theta_W m_Z^2 \frac{v^2}{4}\ell_8^B$	$i\tilde{B}_{\mu\nu}(\partial_\sigma W_I^{\sigma\mu})(\Phi^\dagger\tau_I D^\nu\Phi)$	h_3^Z

Table 1: Parameters determined in this study, corresponding Lagrangian operators in the models of references [2] and [5], and (where appropriate) related on-shell parameters: a) Coefficients of lowest dimension operators contributing to ZZ and $Z\gamma^*$ production or to $Z\gamma^*$ and $Z\gamma$ production; b) Coefficients of lowest dimension operators affecting only the $V^0 Z\gamma^*$ vertices; c) Coefficients of $SU(2)\times U(1)$-conserving operators according to i) the Gounaris-Layssac-Renard constraints and ii) the Alcaraz constraints. The constraints are given in the text. The vertices $V_1^0 V_2^0 V_3^0$ affected by these operators (without distinguishing the V_i^0 as on- or off-mass-shell) are indicated in column 1. The fields Z_μ, F_μ, B_μ and W_μ represent the Z, photon, $U(1)_Y$ and $SU(2)_L$ fields, respectively; $\tilde{Z}_{\mu\nu}$, $\tilde{F}_{\mu\nu}$ and $\tilde{B}_{\mu\nu}$ are the contractions of the respective field tensors with the four-dimensional antisymmetric tensor; Φ is the Higgs field and v its vacuum expectation value, D represents the covariant derivative and τ_I are the Pauli matrices.

state photon is on-shell. In this channel, the kinematic region with high photon energy and large photon polar angle is most sensitive to the anomalous couplings, and in this region the anomalous interactions give rise to a change in the total rate and to an enhancement of the production of longitudinally polarized Z bosons. Our analysis covers two reactions to which the diagrams describing $Z\gamma$ production provide the dominant contribution: $e^+e^- \to \nu\overline{\nu}\gamma$, in which the observed number of events is compared with the number predicted from the total cross-section for this process, and $e^+e^- \to q\bar{q}\gamma$, in which the observed distribution of the decay polar angle $\alpha^\star$ of the Z in its rest frame is compared with predictions derived from the differential distribution $d\sigma/d\cos\alpha^\star$. The present analysis, using data from LEP2 at energies ranging from 189 to 208 GeV, corresponds to a total integrated luminosity of about 594 pb^{-1}. Previous DELPHI results on this channel can be found in [6]; they used data with energies up to $\sqrt{s} = 172$ GeV, and the limits were obtained using an analysis based only on the value of the observed total cross-section.

The total ZZ cross-section is also sensitive to the anomalous couplings, and the sensitivity increases strongly with $\sqrt{s}$. Large interference between Standard Model and anomalous amplitudes arises for CP-conserving couplings (especially for f_5^Z) when one considers the differential cross-section $d\sigma/d\cos\theta_Z$, where θ_Z is the Z production angle with respect to the beam axis. The analysis reported here is based on a study of this differential distribution in the LEP2 data in the energy range 183 to 208 GeV. DELPHI has previously reported a study of the ZZ production cross-section in all visible $f_1\bar{f}_2f_3\bar{f}_4$ final states in these data [7]. The same sets of identified events have been used in the present analysis, with the exception of the $q\bar{q}\tau^+\tau^-$, $\tau^+\tau^-\nu\bar{\nu}$ and $l^+l^-l^+l^-$ channels, which are not used.

In a separate publication [8], DELPHI has studied $Z\gamma^*$ production in the same LEP2 data as used for the channels described above, reporting on a comparison of the cross-section for $Z\gamma^*$ production in various channels with Standard Model predictions. We use the samples identified in [8] in the $q\bar{q}e^+e^-$ and $q\bar{q}\mu^+\mu^-$ final states in the present analysis, which thus represents an interpretation of this data for the first time in terms of possible anomalous gauge couplings. The data were examined as a function of the bidimensional ($M_{l^+l^-}$, $M_{q\bar{q}}$) mass distribution, requiring one of them to be in the region of the Z mass, and they were also divided into two regions of the l^+l^- polar angle with respect to the beam direction (equivalent to the variable θ_Z used in the analysis of ZZ events).

Limits on anomalous neutral gauge couplings in the $Z\gamma$ and ZZ final states have been reported by other LEP experiments; recent published results may be found in the papers listed in [9].

2 Experimental details and analysis

Events were recorded in the DELPHI detector. Detailed descriptions of the DELPHI components can be found in [10] and the description of its performance, as well as of the trigger system and of the luminosity monitor, can be found in [11]. For LEP2 operations, the vertex detector was upgraded [12], and a set of scintillation counters was added to veto photons in blind regions of the electromagnetic calorimetry, at polar angles around $\theta = 40°$ and $\theta = 90°$. The performance of the detector was simulated using the program DELSIM [11], which was interfaced to the programs used in the generation of Monte Carlo events and to the programs used to simulate the hadronization of quarks from Z

and γ^* decay or from background processes. During the year 2000, one sector (1/12) of the time projection chamber, DELPHI's main tracking device, was inactive for about a quarter of the data-taking period. The effect of this was taken into account in the detector simulation and in the determination of cross-sections from the data.

The selection of events in the three physical final states, $Z\gamma$, ZZ and $Z\gamma^*$, considered in this paper, and the simulation of the processes contributing to signals and backgrounds, is described in the following subsections. In the case of the ZZ and $Z\gamma^*$ samples, the reader is referred to recent DELPHI publications on the production of these final states (references [7, 8], respectively) for a full description of the event selection procedures. The event samples used in the present analysis of these two final states have been selected using essentially identical procedures to those described in [7, 8], and cover the same energy range (183 - 208 GeV). These procedures are summarized, respectively, in sections 2.2 and 2.3 below, and any changes from the methods described in [7, 8] are mentioned. DELPHI has also reported a study of events observed at LEP2 in which only photons and missing energy were detected [13]. The present analysis uses data in the part of the kinematic region covered in [13] in which a high energy photon is produced at a large angle with respect to the beam direction; data in the energy range 189 - 208 GeV have been used. The selection procedures specific to this final state as well as to that in which a quark-antiquark pair is produced, rather than missing energy, are described in section 2.1 below.

In the final year of LEP running, data were taken over a range of energies from 205 to 208 GeV. The values of the centre-of-mass energy quoted in the descriptions below for that year correspond to the averages for the data samples collected.

2.1 The $Z\gamma$ final state

The selection procedure for $Z\gamma$ production in the kinematic region with greatest sensitivity to anomalous gauge couplings concentrated on a search for events with a very energetic photon in the angular range $45^\circ < \theta < 135^\circ$, where θ is the polar angle with respect to the beam direction. This angular region is covered by DELPHI's barrel electromagnetic calorimeter, the High Density Projection Chamber (HPC). The search was conducted in events with two final state topologies: $\nu\overline{\nu}\gamma$ and $q\bar{q}\gamma$.

The $\nu\overline{\nu}\gamma$ sample was selected from events with a detected final state containing only a single photon. Its energy was required to be greater than 50 GeV and only photons in the range covered by the HPC, $45^\circ < \theta_\gamma < 135^\circ$, where θ_γ is the polar angle of the photon, were accepted. No tracks or hits were allowed in DELPHI's main tracking detector, the Time Projection Chamber. It was also required that no electromagnetic showers were present in the forward electromagnetic calorimeter and the luminosity monitor, and a second shower in the HPC was accepted only if it was within 20° of the first one. Cosmic ray events were suppressed by requiring that any signal in the hadronic calorimeter be in the same angular region as the signal in the electromagnetic calorimeter, and that the electromagnetic shower point towards the beam collision point within an angle of 15°. The expected numbers of events were calculated using the generators NUNUGPV, based on [14], and KORALZ [15], interfaced to the full DELPHI simulation program, DELSIM. The trigger efficiency was measured from the data. From these simulations, the efficiency for detecting $\nu\overline{\nu}\gamma$ events in the kinematic region considered here was estimated to be in the region of 50%, independent of the centre-of-mass energy. Contributions from

background sources to this channel were estimated to be negligible. The results obtained applying these criteria are shown in table 2. The distribution of the energy of identified photons normalized to the beam energy, E_γ/E_{beam}, in the data collected in the $\nu\overline{\nu}\gamma$ channel before imposing the cut at $E_\gamma = 50$ GeV is shown in figure 2a), and compared with the expectation of the Standard Model.

$\sqrt{s}$ (GeV)	Integrated luminosity (pb^{-1})	Selected data	Total predicted events
188.6	154.7	87	89.2
191.6	25.1	14	13.1
195.5	76.2	32	37.5
199.5	83.1	45	38.5
201.6	40.6	20	18.2
206.1	214.6	98	102.3
Total	594.3	296	298.8

Table 2: $\nu\overline{\nu}\gamma$ final state: Integrated luminosity and numbers of observed and expected events at each energy, $\sqrt{s}$.

In the selection of events in the $q\bar{q}\gamma$ channel, the same requirements were imposed on photon candidates, $E_\gamma > 50$ GeV and $45° < \theta_\gamma < 135°$, while, in addition, events were required to have six or more charged particle tracks, each with length greater than 20 cm, momentum greater than 200 MeV/c, polar angle between 10° and 170°, and transverse and longitudinal impact parameters at the interaction point of less than 4 cm. The total charged energy in the event was required to exceed 0.10 of the centre-of-mass energy and the effective energy of the collision [16], $\sqrt{s'}$, was required to satisfy $\sqrt{s'}$ <130 GeV. Jets were reconstructed using the LUCLUS [17] algorithm and the event forced into a two-jet configuration. The identified photon was required to be isolated from the nearest jet axis by at least 20°. The efficiency, purity and the expected numbers of events from other processes were computed using events generated with PYTHIA [17], relying on JETSET 7.4 [17] for quark fragmentation, and interfaced to the full DELPHI simulation program, DELSIM. From these simulations, the efficiency for detecting $q\bar{q}\gamma$ events in the kinematic region considered here was estimated to be in the region of 77%, independent of the centre-of-mass energy. The results obtained applying this procedure are shown in table 3.

Summing over all energy points, totals of 296 and 1581 events were observed in the $\nu\overline{\nu}\gamma$ and $q\bar{q}\gamma$ channels, respectively. These numbers may be compared with the totals expected from simulated production of these final states by Standard Model processes: 298.8 events in $\nu\overline{\nu}\gamma$, and 1601.5 events in $q\bar{q}\gamma$.

In the $\nu\overline{\nu}\gamma$ channel, values of the gauge boson coupling parameters were derived by comparing the observed number of events with that predicted from the total cross-section for this process, while in the $q\bar{q}\gamma$ channel a fit was performed to the distribution of the decay angle, $\alpha^\star$, of the Z in its rest frame. The value of $\alpha^\star$ was estimated from the directions of the vectors in the laboratory frame $\mathbf{p}_\gamma$ and $\mathbf{p_i}$ of the reconstructed photon and jets ($i = 1, 2$), respectively, as:

$$\cot\alpha^\star = \gamma\left(\cot\alpha_1 - \frac{\beta}{\sin\alpha_1}\right), \tag{6}$$

$\sqrt{s}$ (GeV)	Integrated luminosity (pb^{-1})	Selected data	Total predicted events	Expected background
188.6	154.3	454	467.3	14.9
191.6	25.4	79	75.0	2.6
195.5	77.1	203	214.1	5.8
199.5	84.2	208	225.5	5.9
201.6	40.6	130	104.5	2.8
205.9	218.8	507	515.1	13.9
Total	600.4	1581	1601.5	45.9

Table 3: $q\bar{q}\gamma$ final state: Integrated luminosity and numbers of observed and expected events at each energy, $\sqrt{s}$.

$$\text{with} \quad \beta = \frac{\sin(\alpha_1+\alpha_2)}{\sin\alpha_1+\sin\alpha_2}, \quad \cos\alpha_{\rm i} = -\frac{\mathbf{p}_\gamma\cdot\mathbf{p}_{\rm i}}{|\mathbf{p}_\gamma|\cdot|\mathbf{p}_{\rm i}|} \quad \text{and} \quad \gamma = \frac{1}{\sqrt{1-\beta^2}}\,. \tag{7}$$

The distribution of $\cos\alpha^\star$ for the data selected in the $q\bar{q}\gamma$ channel is shown in figure 2b) and compared with the predictions of the Standard Model and of a non-standard scenario with $h_3^\gamma = \pm 0.2$. The predictions for non-zero neutral gauge boson couplings were made by reweighting the simulated samples produced according to the Standard Model with the calculations of Baur [18][3].

2.2 The ZZ final state

The study of the triple gauge boson vertex in ZZ production has used the samples of events selected by DELPHI in the $q\overline{q}q\overline{q}$, $q\bar{q}\mu^+\mu^-$, $q\bar{q}e^+e^-$, $q\bar{q}\nu\bar{\nu}$, $\mu^+\mu^-\nu\bar{\nu}$ and $e^+e^-\nu\bar{\nu}$ final states. The procedures used have been described fully in [7]; we give here a brief summary of the methods used in the selection of events in each of these final states, and provide a table of the total numbers of events observed and expected for production of each of them by Standard Model processes.

The $ZZ \to q\overline{q}q\overline{q}$ process represents 49% of the ZZ decay topologies and produces four or more jets in the final state. After a four-jet preselection, the ZZ signal was identified within the large background from WW and $q\bar{q}\gamma$ production by evaluating a probability that each event came from ZZ production, based on invariant mass information, on the b-tag probability per jet and on topological information.

The process $e^+e^- \to q\bar{q}l^+l^-$ has a branching ratio from ZZ production of 4.7% per lepton flavour. High efficiency and high purity were attained with a cut-based analysis using the clear experimental signature provided by the two leptons, which are typically well isolated from all other particles. The on-shell ZZ sample was selected by applying simultaneous cuts on the masses of the l^+l^- pair, on the remaining hadronic system and on their sum.

The decay mode $q\bar{q}\nu\bar{\nu}$ represents 28% of the ZZ final states. The signature of this decay mode is a pair of rather acoplanar jets with visible and recoil masses compatible with the Z mass. The most difficult backgrounds arise from single resonant $We\nu_e$ production, from WW production where one of the W bosons decays into $\tau\nu_\tau$, and from $q\bar{q}$ events

[3]The code used was modified by a factor i according to the correction suggested by Gounaris *et al* [19].

accompanied by energetic isolated photons escaping detection. The selection of events was made using a combined discriminant variable obtained with an Iterative Discriminant Analysis program (IDA) [20].

The final state $l^+l^-\nu\bar{\nu}$ has a branching ratio from ZZ production of 2.7% per lepton flavour. Events with $l \equiv \mu, e$ were selected with a sequential cut-based analysis. The on-shell ZZ sample was selected from the events assigned to this final state by applying cuts on the masses of the l^+l^- pair and of the system recoiling against it. The most significant background in the sample is from WW production with both Ws decaying leptonically.

In the estimation of the expected numbers of events in all the final states discussed above, processes leading to a four-fermion final state were simulated with EXCALIBUR [21], with JETSET 7.4 used for quark fragmentation. Amongst the background processes leading to the final state toplogies described above, GRC4F [22] was used to simulate $We\nu$ production, PYTHIA for $q\bar{q}(\gamma)$, KORALZ for $e^+e^-\mu^+\mu^-$ and $e^+e^-\tau^+\tau^-$, BHWIDE [23] for $e^+e^-e^+e^-$, and TWOGAM [24] and BDK [25] for two-photon processes.

The presence of anomalous neutral triple gauge boson couplings in the data samples described above was investigated by studying the distribution of the Z production polar angle, $\cos\theta_Z$. The reconstruction of θ_Z is free from ambiguity for all channels except $q\overline{q}q\overline{q}$, where the indistinguishability of the jets leads to three possible jet-jet pairs, each of which could come from ZZ decay. A 5-constraint kinematic fit was performed on each of these combinations, imposing four-momentum conservation and imposing equality of the masses of the two jet pairs. The fit with the minimum value of χ^2 was retained and the value of $\cos\theta_Z$ evaluated from the fitted jet directions.

Figure 3 shows the $\cos\theta_Z$ distribution for a high purity sample of ZZ data, defined in table 4, together with the Standard Model expectations and the distributions predicted for values of $f_5^Z = \pm 1.5$. The samples of $q\overline{q}q\overline{q}$ and $q\bar{q}\nu\bar{\nu}$ events displayed in the figure and described in the table were selected imposing stringent cuts on the probabilistic variables used in these channels ($q\overline{q}q\overline{q}$ probability > 0.55, and $q\bar{q}\nu\bar{\nu}$ IDA variable > 3), so as to suppress the background levels present in the samples. In table 4, the quoted values for the selection efficiency are defined as the fraction of events of the four-fermion final state listed in the first column of the table present in the selected sample.

Channel	Integrated luminosity (pb^{-1})	Selected data	Total predicted events	Expected background	Selection efficiency
$q\overline{q}q\overline{q}$	665.1	76	69.4	22.1	0.18
$q\bar{q}\mu^+\mu^-$	665.3	21	22.0	1.1	0.86
$q\bar{q}e^+e^-$	665.3	19	23.7	2.6	0.73
$q\bar{q}\nu\bar{\nu}$	639.0	45	55.5	22.3	0.21
$l^+l^-\nu\bar{\nu}$	665.3	10	8.9	4.7	0.30
Total	–	171	179.5	52.8	–

Table 4: ZZ production: Integrated luminosity, numbers of observed and expected events and estimated selection efficiency for each topological final state, summed over all energies.

In the determination of the coupling parameters, extended maximum likelihood fits were made to the distribution of $\cos\theta_Z$ for data from the channels selected with cut-based analyses ($q\bar{q}l^+l^-$ and $q\bar{q}\nu\bar{\nu}$), while for the channels selected using probabilistic methods

($q\overline{q}q\overline{q}$ and $q\bar{q}\nu\bar{\nu}$), a simultaneous fit was made to the distributions of $\cos\theta_Z$ and of the discriminant variable (the ZZ probability for $q\overline{q}q\overline{q}$ and the IDA output variable for $q\bar{q}\nu\bar{\nu}$), without applying any cuts to the values of these variables.

The predictions for non-zero neutral gauge boson couplings were made by reweighting the simulated samples produced according to the Standard Model with the calculations of the DELTGC [26] event generator, which adds the amplitude from hypothesized neutral triple gauge boson vertices to all the other amplitudes contributing to the production of any four-fermion final state.

2.3 The $Z\gamma$* final state

In a separate publication [8], DELPHI has reported on a study of $Z\gamma^*$ production in LEP2 data, and in particular on a comparison of the observed cross-section with Standard Model predictions, using data from a variety of four-fermion final state topologies involving both hadronic and leptonic Z decay modes. In the present analysis, we interpret data in the $q\bar{q}\mu^+\mu^-$ and $q\bar{q}e^+e^-$ final states in terms of possible anomalous triple gauge boson interactions. These two channels are chosen because the two final state leptons are typically well isolated from all other particles, allowing such events to be selected with high efficiency over the whole region of γ^* mass. Events with either the l^+l^- or the $q\bar{q}$ invariant mass in the vicinity of the Z mass and the other invariant mass not in the Z region were then used in the estimation of possible anomalous gauge coupling parameters; the precise definition of the signal region is shown graphically in figure 4. Full details of the selection procedure are given in [8]; a summary of the main features follows.

Events containing hadronic material with total charged energy above $0.3\sqrt{s}$ and at least two lepton candidates of the same flavour and opposite charge were selected. All particles except the lepton candidates were clustered into jets and a kinematic fit requiring four-momentum conservation was applied. At least one of the two lepton candidates was required to satisfy strong lepton identification criteria, while softer requirements were specified for the second. The final event selection was made using cuts in two discriminating variables: P_t^{min}, the lesser of the transverse momenta of the lepton candidates with respect to their nearest jet, and the χ^2 per degree of freedom of the kinematic fit. The backgrounds in the selected samples from final states other than $q\bar{q}\mu^+\mu^-$ and $q\bar{q}e^+e^-$ are small, coming mainly from $q\bar{q}\tau^+\tau^-$, WW and, in the case of $q\bar{q}e^+e^-$, from $q\bar{q}(\gamma)$ production.

The simulation of processes leading to four-fermion final states was done with WPHACT [27], using the JETSET model for quark hadronization, while the $q\bar{q}(\gamma)$ final state was simulated with the KK2f [28] model. Both of these programs were interfaced to the DELPHI simulation program, DELSIM.

Table 5 summarizes the selection procedures outlined above, showing, for the sum of data over all energy points, the total integrated luminosity, the numbers of observed and predicted events and the estimated selection efficiency (defined as for the ZZ sample described in section 2.2 above) for each topological final state.

In the determination of the coupling parameters, bidimensional distributions of the selected events in the plane of the masses of the two fermion-antifermion pairs were used, defining a small number of bins of unequal size, but containing roughly equal predicted numbers of events. Different bin definitions were made for the $q\bar{q}\mu^+\mu^-$ and $q\bar{q}e^+e^-$ channels, corresponding to those used by DELPHI in [8] in the determination of the $Z\gamma^*$

Channel	Integrated luminosity (pb^{-1})	Selected data	Total predicted events	Expected background	Selection efficiency
$q\bar{q}\mu^+\mu^-$	666.7	35	36.7	3.4	0.53
$q\bar{q}e^+e^-$	666.7	39	36.3	6.0	0.44

Table 5: $Z\gamma^*$ production: Integrated luminosity, numbers of observed and expected events and estimated selection efficiency for each topological final state, summed over all energies.

cross-section; they are shown in figure 4. In [8], each of the mass bins defined for the $q\bar{q}e^+e^-$ event sample was further divided into two angular regions, ($40° < \theta_{ll} < 140°$) and ($\theta_{ll} < 40°$ or $\theta_{ll} > 140°$), where θ_{ll} is the polar angle of the final state e^+e^- system with respect to the beam direction. These angular regions correspond to DELPHI's barrel and endcap regions, respectively. In the present analysis, we have extended this division to apply to muon as well as electron pairs in the $q\bar{q}l^+l^-$ final states, as the Feynman diagrams containing neutral gauge boson couplings are s-channel diagrams (see figure 1) and are hence expected to populate the large-angle region more significantly. Binned likelihood fits to the couplings were then made with the bins in $(M_{l^+l^-}, M_{q\bar{q}})$ and $\theta_{l^+l^-}$ thus defined.

As described in section 1.1, data from the $Z\gamma^*$ final state were used in the determination of all the coupling parameters studied in this paper; however, the $Z\gamma^*$ data play a statistically significant role only in the determination of the coefficients of the $d = 8$ operators which affect solely the $V^0Z\gamma^*$ vertices. (This point is discussed again in section 3.2 below). Figure 5 shows the distributions of $M_{l^+l^-}$ ($l \equiv \mu, e$) and of $M_{q\bar{q}}$ in the combined $q\bar{q}\mu^+\mu^-$ and $q\bar{q}e^+e^-$ experimental data, and compares them with the expectations of the Standard Model and of a non-standard scenario with a contribution, $\tilde{\ell}_4^{ZZ\gamma} m_Z^4 = 3.4$, from the $d = 8$ operator $\tilde{\mathcal{O}}_4^{ZZ\gamma}$ defined in table 1.

As in the case of the ZZ final state previously described, the predictions for non-zero neutral gauge boson couplings in the $Z\gamma^*$ data were made by reweighting the simulated samples produced according to the Standard Model with the calculations of DELTGC.

3 Results

In this section the results of our study are presented, expressed in terms of the parameters listed in table 1 describing the neutral triple gauge boson effective Lagrangian. In summary, these parameters represent a): the coefficients of the lowest dimension operators contributing either to ZZ and $Z\gamma^*$ production or to $Z\gamma^*$ and $Z\gamma$ production, each of which becomes equal in the on-shell ZZ or $Z\gamma$ limit to one of the on-shell coefficients f_i^V or h_i^V; b): the coefficients of the lowest dimension operators affecting only the $V^0Z\gamma^*$ vertex; and c): the coefficients of the $SU(2) \times U(1)$-conserving operators describing the $V_1^0V_2^0V_3^0$ vertex in i) the Gounaris-Layssac-Renard and ii) the Alcaraz formulations. (The labels a), b), c) refer to table 1).

The results of one-parameter fits to the data are shown in table 6 and figures 6-10. In all cases, the values quoted are derived from likelihood distributions based on fits to the data in the $Z\gamma$, ZZ and $Z\gamma^*$ channels described in sections 2.1, 2.2 and 2.3 above, summing the distributions from different channels where appropriate. In each fit, the values of the other parameters were set to zero, their Standard Model value. For

reference, we summarize here the composition of the likelihood function from each of the final states used in the analysis, described in more detail in the sections above: In the $Z\gamma \to \nu\overline{\nu}\gamma$ channel, the number of events with a high energy photon emitted at large polar angle was used in the fit, while in the $Z\gamma \to q\bar{q}\gamma$ channel the fit was performed to the distribution of the decay angle of the Z in its rest frame. In the channels $ZZ \to q\bar{q}l^+l^-$ and $ZZ \to l^+l^-\nu\bar{\nu}$ the distribution of the Z production angle was fitted; in $ZZ \to q\overline{q}q\overline{q}$ and $ZZ \to q\bar{q}\nu\bar{\nu}$ simultaneous fits were made to the Z production angle and, respectively, to the event probability or discriminant variable distributions. In the $Z\gamma^*$ channels studied ($Z\gamma^* \to q\bar{q}\mu^+\mu^-$ and $Z\gamma^* \to q\bar{q}e^+e^-$) the likelihood was evaluated in bins of $q\bar{q}$ or l^+l^- mass and of the polar angle of the detected l^+l^- system.

3.1 Systematic errors

The errors and limits results shown in table 6 and figures 6-10 include contributions from both statistical and systematic effects. Several sources of systematic error were considered for each of the final states included in the study. These are described below.

In the $\nu\overline{\nu}\gamma$ and $q\bar{q}\gamma$ channels contributing to $Z\gamma$ production, uncertainties of $\pm 1\%$ were assumed in the values assumed for the Standard Model production cross-sections, and an experimental uncertainty of $\pm 1\%$ was assumed for the calibration of the electromagnetic calorimeter. The effect of an uncertainty of $\pm 1\%$ in the luminosity measurement was also computed, while the uncertainties in the calculations arising from the finite simulated statistics in signal and background channels were found to be negligible in both channels. In the $\nu\overline{\nu}\gamma$ channel, the error due to the uncertainty of $\pm 3\%$ in the trigger efficiency was calculated. In the $q\bar{q}\gamma$ channel, the uncertainty in the use of PYTHIA as the hadronization model was taken into account by comparing events simulated with PYTHIA and HERWIG [29]; this gave rise to an estimated systematic error of $+1.7\%$ from this source. In the combination of data at different energies, all the above effects were considered as correlated. The resulting overall systematic error in the coupling parameters was found to be of the order of 30% of the statistical errors in the case of h_1^Z and h_3^Z, about 50% of the statistical error for h_1^γ, and of the same order as the statistical error for h_3^γ.

A full description of the treatment of systematic effects in the channels contributing to ZZ production has been given in [7]. In the $q\overline{q}q\overline{q}$ channel, the dominant effect arises from uncertainties in the modelling of the main source of background, namely production of the $q\bar{q}(\gamma)$ final state, when the subsequent hadronization of the quarks gives rise to several jets. In the present study, the effect of this background was estimated by assuming an uncertainty of $\pm 5\%$ in the $q\bar{q}(\gamma)$ production cross-section. In the $q\bar{q}l^+l^-$ channel, the dominant systematic effect relevant to the present study comes from the uncertainty in the efficiency for selecting $q\bar{q}e^+e^-$ and $q\bar{q}\mu^+\mu^-$ events, taken to be $\pm 3\%$. In addition, in the $q\bar{q}e^+e^-$ channel a systematic error of $\pm 1.6\%$ was estimated to arise from the uncertainty in the calculation of the background level. In the $q\bar{q}\nu\bar{\nu}$ channel, as in $q\overline{q}q\overline{q}$, the main source of systematic error arises from modelling of the $q\bar{q}(\gamma)$ background, in this case corresponding to the kinematic region with large missing energy, and hence low visible $q\bar{q}$ energy. A study of the energy flow in this region using events at the Z peak allowed a determination of the effect of this uncertainty in the present analysis; it gives rise to systematic errors in the coupling parameters of order 5% - 10% of the values of the statistical errors. Another, comparable source of systematic error in this channel comes from the uncertainties in the cross-sections for the dominant background channels, particularly

Parameter	Channels used	Value	95% Confidence interval	Related on-shell coefficient
a)				
$\tilde{\ell}_1^{ZZZ} m_Z^2$	ZZ $Z\gamma^*$	$+0.03^{+0.23}_{-0.26}$	$[-0.40, +0.42]$	f_4^Z
$\ell_1^{ZZZ} m_Z^2$	ZZ $Z\gamma^*$	$+0.11^{+0.25}_{-0.26}$	$[-0.38, +0.62]$	f_5^Z
$\tilde{\ell}_3^{ZZ\gamma} m_Z^2$	ZZ $Z\gamma^*$	$+0.03^{+0.13}_{-0.15}$	$[-0.23, +0.25]$	f_4^γ
$\ell_2^{ZZ\gamma} m_Z^2$	ZZ $Z\gamma^*$	$-0.07^{+0.32}_{-0.26}$	$[-0.52, +0.48]$	f_5^γ
$\tilde{\ell}_1^{ZZ\gamma} m_Z^2$	$Z\gamma$ $Z\gamma^*$	$+0.08^{+0.10}_{-0.23}$	$[-0.23, +0.24]$	h_1^Z
$\ell_1^{ZZ\gamma} m_Z^2$	$Z\gamma$ $Z\gamma^*$	$-0.15^{+0.25}_{-0.09}$	$[-0.31, +0.17]$	h_3^Z
$\tilde{\ell}_1^{Z\gamma\gamma} m_Z^2$	$Z\gamma$ $Z\gamma^*$	$+0.04^{+0.07}_{-0.14}$	$[-0.14, +0.14]$	h_1^γ
$\ell_1^{Z\gamma\gamma} m_Z^2$	$Z\gamma$ $Z\gamma^*$	$+0.001^{+0.023}_{-0.024}$	$[-0.049, +0.045]$	h_3^γ
b)				
$\tilde{\ell}_4^{ZZ\gamma} m_Z^4$	$Z\gamma^*$ ZZ	$+0.41^{+0.93}_{-1.39}$	$[-1.67, +1.92]$	–
$\ell_2^{Z\gamma\gamma} m_Z^4$	$Z\gamma^*$ ZZ	$+0.14^{+0.26}_{-0.33}$	$[-0.49, +0.61]$	–
c) i)				
$-\cot\theta_W m_Z^2 \frac{v^2}{4} \tilde{\ell}_{SU(2)\times U(1)}$	$Z\gamma$ $Z\gamma^*$ ZZ	$+0.02^{+0.08}_{-0.11}$	$[-0.13, +0.13]$	h_1^γ
$-\cot\theta_W m_Z^2 \frac{v^2}{4} \ell_{SU(2)\times U(1)}$	$Z\gamma$ $Z\gamma^*$ ZZ	$+0.004^{+0.023}_{-0.024}$	$[-0.045, +0.047]$	h_3^γ
ii)				
$-\cot\theta_W m_Z^2 \frac{v^2}{4} \tilde{\ell}_8^A$	$Z\gamma$ $Z\gamma^*$ ZZ	$+0.04^{+0.06}_{-0.13}$	$[-0.14, +0.14]$	h_1^γ
$-\cot\theta_W m_Z^2 \frac{v^2}{4} \ell_8^A$	$Z\gamma$ $Z\gamma^*$ ZZ	$+0.001^{+0.023}_{-0.024}$	$[-0.049, +0.045]$	h_3^γ
$-\cot\theta_W m_Z^2 \frac{v^2}{4} \tilde{\ell}_8^B$	$Z\gamma$ $Z\gamma^*$ ZZ	$+0.07^{+0.10}_{-0.22}$	$[-0.23, +0.24]$	h_1^Z
$-\cot\theta_W m_Z^2 \frac{v^2}{4} \ell_8^B$	$Z\gamma$ $Z\gamma^*$ ZZ	$+0.02^{+0.10}_{-0.24}$	$[-0.30, +0.18]$	h_3^Z

Table 6: Results of the study of neutral gauge couplings. For each of the parameters listed in table 1, the table shows the experimental channels used, the parameter value with maximum likelihood and its 1 S.D. errors, and the 95% confidence limits. The right-hand-most column indicates the parameter which, in the on-shell limit, is equal to the parameter determined. In the determination of any one coupling, the values of all the others were held at their Standard Model values. The errors and limits shown include both statistical and systematic effects: a) Coefficients of lowest dimension operators contributing either to ZZ and $Z\gamma^*$ production or to $Z\gamma$ and $Z\gamma^*$ production; b) Coefficients of lowest dimension operators affecting only the $V^0 Z\gamma^*$ vertices; c) Coefficients of $SU(2) \times U(1)$-conserving operators according to i) the Gounaris-Layssac-Renard constraints and ii) the Alcaraz constraints (see text, section 1.1).

$We\nu$ production. Systematic effects in the $l^+l^-\nu\bar{\nu}$ channels were found to be negligible. In addition, the effects of uncertainties of $\pm 2\%$ in the overall ZZ cross-section and of $\pm 1\%$ in the luminosity measurement were considered. The combined effect of all the systematic uncertainties in the channels contributing to ZZ production is small, typically $\sim 15\%$ of the statistical errors.

The systematic uncertainties in the study of the $q\bar{q}e^+e^-$ and $q\bar{q}\mu^+\mu^-$ channels contributing to $Z\gamma^*$ production have been described in [8]. Several effects, including uncertainties in lepton identification, the effect of limited simulated data and, in the $q\bar{q}e^+e^-$ channel, identification of fake electrons coming from background channels, combine to give a systematic error on the efficiency to select $q\bar{q}e^+e^-$ and $q\bar{q}\mu^+\mu^-$ events of $\pm 5\%$ and a relative uncertainty in the background level of $\pm 15\%$. In addition, a systematic error of $\pm 1\%$ in the luminosity measurement was assumed. The overall effect of these systematic uncertainties in the determination of the coupling parameters is small in comparison with the statistical errors; in the case of the parameters listed in table 6b) they amount to $\sim$15% and $\sim$5% of the statistical errors for ${\ell_2}^{Z\gamma\gamma}$ and ${\tilde{\ell}_4}^{ZZ\gamma}$, respectively.

In the combination of data from the different final states, $Z\gamma$, ZZ and $Z\gamma^*$, all the systematic effects listed above were treated as uncorrelated except those arising from the uncertainty in the luminosity measurement.

3.2 Discussion

A few comments may be made on the results shown in table 6 and figures 6-10.

All the results are compatible with the Standard Model expectation of the absence of neutral triple gauge boson couplings. The results shown in table 6a) and figures 6 and 7 demonstrate this conclusion in the effective Lagrangian model of reference [2] for the $d = 6$ operators contributing to $Z\gamma$ and $Z\gamma^*$ production or to ZZ and $Z\gamma^*$ production. The contribution of the data from the $Z\gamma^*$ channels to the precision determined for these parameters is small (as has been predicted from simulated studies [5]): determination of these parameters using only $Z\gamma^*$ data leads to precisions poorer by factors of $\sim 3-7$ than those shown in the table. (This effect is observed most strongly in the case of the determination of h_3^γ, where the interference in the squared matrix element between the anomalous and Standard Model amplitudes leads to a relatively precise determination of this parameter). Thus these results, with negligible changes, may also be interpreted in terms of the parameters h_i^V and f_i^V of on-shell $Z\gamma$ and ZZ production, listed in the right-hand column of the table, and they may be compared directly with other published results for these on-shell parameters.

The results shown in table 6b) and figure 8 examine the possibility of four-fermion production via an anomalous $V^0Z\gamma^*$ vertex by determining the coefficients of the lowest dimension ($d = 8$) operators in the model of reference [2] which would contribute to such a process. As noted in section 2.3, contributions from these operators affect both the $Z\gamma^*$ and ZZ final states, and both these experimental samples were used in the fits to the data. In this combination of data, the contribution from the $Z\gamma^*$ events to the precision of the fits is of the same order as that from the events in the ZZ sample, in contrast to the situation in the $d = 6$ case discussed in the previous paragraph. The results of the fits show that there is no evidence in the data for a CP-conserving anomalous coupling at the $\gamma^*Z\gamma^*$ vertex or for a CP-violating coupling at the $Z^*Z\gamma^*$ vertex.

The results shown in table 6c) and figures 9 and 10 indicate that there is no evidence in

the data for $SU(2) \times U(1)$-conserving anomalous couplings in the models of references [2] and [5]. Here again, in the combinations of data from different final states, the contributions from $Z\gamma$ production dominate, as can be seen by comparison of the likelihood curves of figure 7 and either figure 9 or figure 10. This arises both because of the sensitivity to h_3^γ noted above and because of the greater statistical contribution from $Z\gamma$ compared to that from ZZ production at LEP2 energies.

4 Conclusions

A study has been performed of the neutral triple gauge boson vertex using DELPHI data from the final states $Z\gamma$, ZZ and $Z\gamma^*$ produced at LEP2. The results have been interpreted in terms of various models of the interaction Lagrangian proposed in the literature. We find no evidence for the production of these states by processes involving neutral triple gauge boson vertices with either one or two off-shell bosons, nor when the data are analyzed in terms of models in which the neutral triple gauge boson vertex is constrained to be $SU(2) \times U(1)$-conserving. These conclusions are in agreement with the predictions of the Standard Model.

References

[1] K. Hagiwara, K. Hikasa, R.D. Peccei and D. Zeppenfeld, Nucl. Phys. **B282** 253 (1987).

[2] G. Gounaris, J. Layssac and F.M. Renard, Phys.Rev. **D62** (2000) 073012.

[3] M. Bilenky, J.L. Kneur, F.M. Renard and D. Schidknecht, Nucl.Phys. **B409** 22 (1993).

[4] G. Gounaris, J.-L. Kneur and D. Zeppenfeld, in *Physics at LEP2*, eds. G. Altarelli, T. Sjöstrand and F. Zwirner, CERN 96-01 Vol.1, 525 (1996).

[5] J. Alcaraz, Phys.Rev. D65 (2002) 075020.

[6] DELPHI Collaboration, W. Adam *et al.*, Phys. Lett. **B380** (1996) 471 ;
DELPHI Collaboration, P. Abreu *et al.*, Phys.Lett. **B423** (1998) 194.

[7] DELPHI Collaboration, J. Abdallah *et al.*, Eur. Phys. J. **C30** (2003) 447.

[8] DELPHI Collaboration, M. Begalli, E. Graziani and M.E. Pol, *$Z\gamma^*$ production in e^+e^- interactions at $\sqrt{s}$ = 183 - 209 GeV*, submitted to ICHEP 2004, Beijing (2004).

[9] ALEPH Collaboration, ALEPH 2001-014 CONF 2001-011 (2001);
L3 Collaboration, P. Achard *et al.*, CERN-EP/2003-034 [hep-ex/0308013] 2003;
L3 Collaboration, P. Achard *et al.*, CERN-PH-EP/2004-014 [hep-ex/0407012] (2004);
OPAL Collaboration G. Abbiendi *et al.*, Eur. Phys. J. **C17** (2000) 553;
OPAL Collaboration, G. Abbiendi *et al.*, Eur. Phys. J. **C32** (2004) 303.

[10] DELPHI Collaboration, P. Aarnio *et al.*, Nucl. Instr. and Meth. **A303** (1991) 233.

[11] DELPHI Collaboration, P. Abreu *et al.*, Nucl. Instr. and Meth. **A378** (1996) 57.

[12] DELPHI Silicon Tracker Group, P. Chochula *et al.*, Nucl. Instr. and Meth. **A412** (1998) 304.

[13] DELPHI Collaboration, J. Abdallah *et al.*, CERN-EP/2003-093 (2003), submitted to Eur. Phys. J.

[14] G. Montagna *et al.*, Nucl. Phys. **B452** (1995) 161.

[15] S. Jadach *et al.*, Comp. Phys. Comm. **79** (1994) 503.

[16] DELPHI Collaboration, P. Abreu *et al.*, Nucl. Instr. and Meth. **A427** (1999) 487.
[17] T.Sjöstrand, *PYTHIA 5.7 / JETSET 7.4*, CERN-TH 7112/93 (1993).
[18] U. Baur and E. Berger, Phys. Rev. **D47** (1993) 4889.
[19] G. Gounaris, J. Layssac and F.M. Renard, Phys.Rev. **D61** (2000) 073013.
[20] T.G.M. Malmgren, Comp. Phys. Comm. **106** (1997) 230;
T.G.M. Malmgren and K.E. Johansson, Nucl. Inst. and Meth. **403** (1998) 481.
[21] F.A. Berends, R. Kleiss and R. Pittau, Comp. Phys. Comm. **85** (1995) 437.
[22] J. Fujimoto *et al.*, Comp. Phys. Comm. **100** (1997) 128.
[23] S. Jadach, W. Placzek and B.F.L. Ward, Phys. Lett. **B390** (1997) 298.
[24] T. Alderweireld *et al.*, CERN-OPEN-2000-141 (2000).
[25] F.A. Berends, P.H. Daverfeldt and R. Kleiss, Comp. Phys. Comm. **40** (1986) 271, 285 and 309.
[26] V.V. Kostyukhin, V.F. Obraztsov and O.P. Yushchenko, *DELTGC - A program for four-fermion calculations*, DELPHI 99-4 PHYS 816 (1999).
[27] E. Accomando and A. Ballestrero, Comp. Phys. Comm. **99** (1997) 270;
E. Accomando, A. Ballestrero and E. Maina, Comp. Phys. Comm. **150** (2003) 166;
A. Ballestrero, R. Chierici, F. Cossutti and E. Migliore, Comp. Phys. Comm. **152** (2003) 175.
[28] S. Jadach, B.F.L. Ward and Z. Was, Comp. Phys. Comm. **130** (2000) 260.
[29] G. Marchesini *et al.*, Comp. Phys. Comm. **67** (1992) 465.

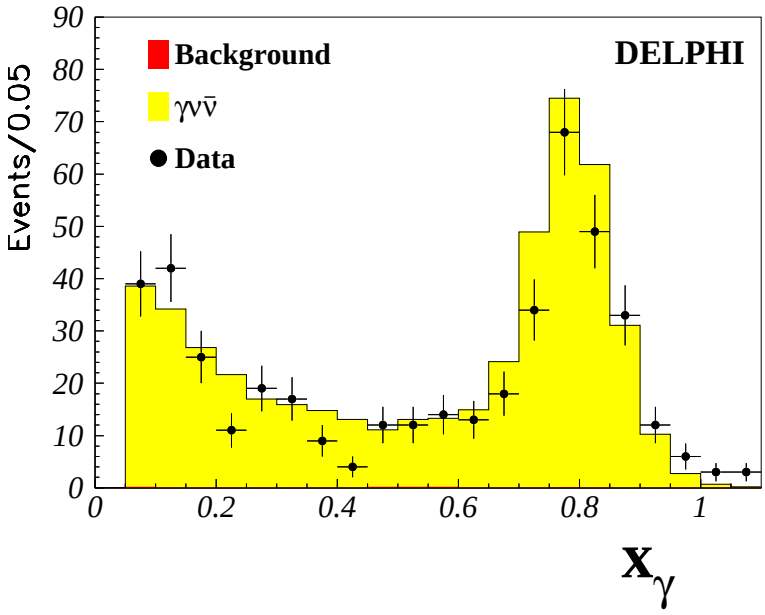

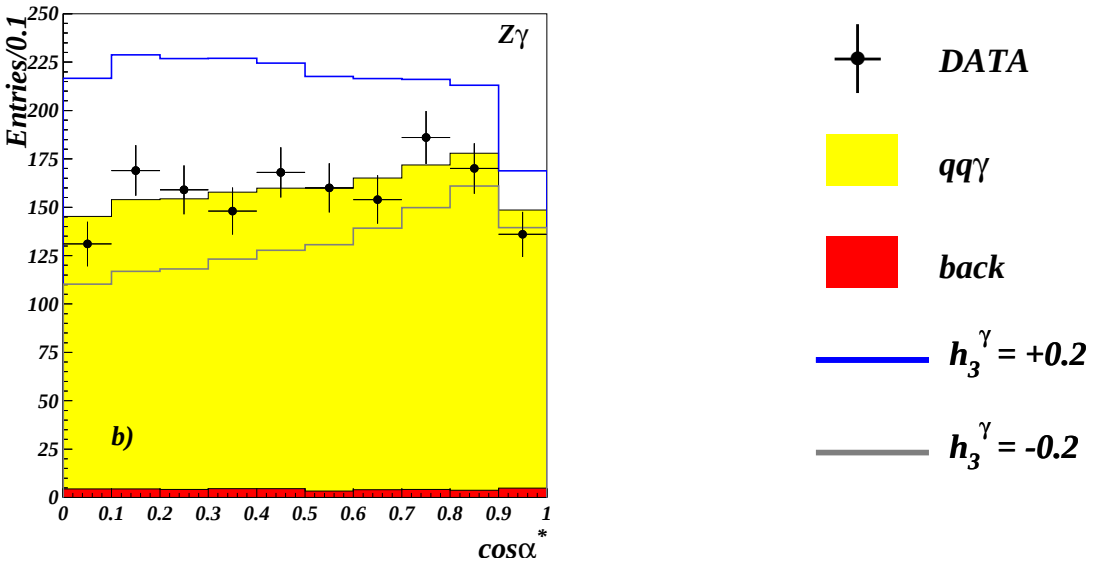

Figure 2: a) Distribution of $x_\gamma = E_\gamma / E_{beam}$, the energy of identified photons normalized to the beam energy in the data in the $\nu\overline{\nu}\gamma$ channel, summed over all energy points. The distribustion is shown before imposing the experimental cut at $E_\gamma = 50$ GeV. The experimental data points are shown by crosses and the shaded histogram shows the predictions of the Standard Model for signal and background. b) Distribution of the decay angle, $\cos\alpha^*$, of the quark (or antiquark) in the Z centre-of-mass frame for data selected in the $q\bar{q}\gamma$ channel. The experimental data points are shown by crosses, the shaded histogram shows the predictions of the Standard Model for signal and background, and the outlined histograms the expectations for values of $h_3^\gamma = \pm 0.2$.

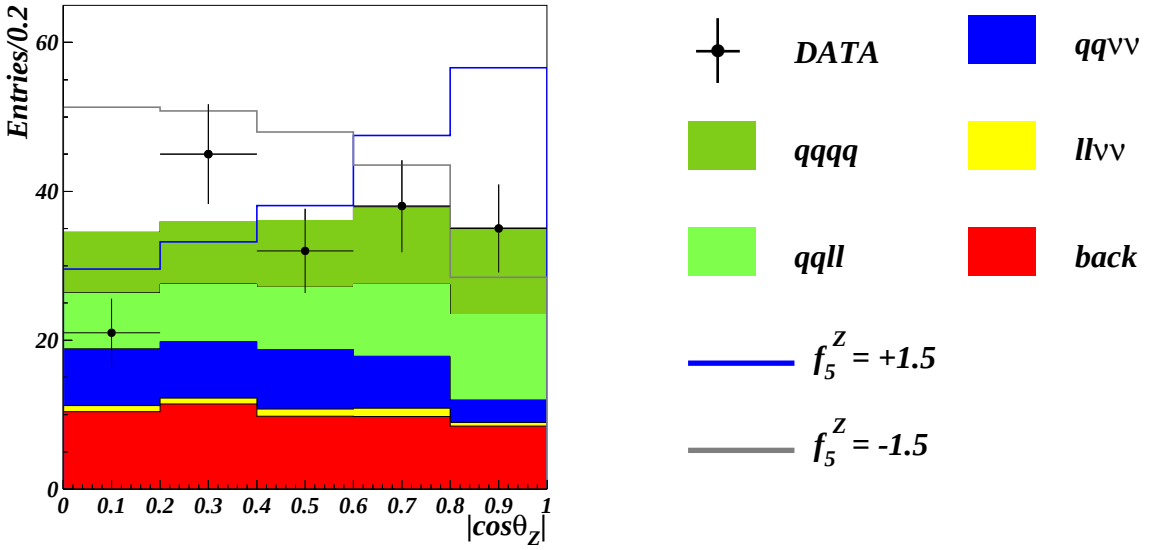

Figure 3: Distribution of the Z polar angle, $\cos\theta_Z$, for data selected in the ZZ channels. The experimental data points are shown by crosses, the shaded histogram shows the predictions of the Standard Model for signal and background, and the outlined histograms the expectations for values of $f_5^Z = \pm 1.5$.

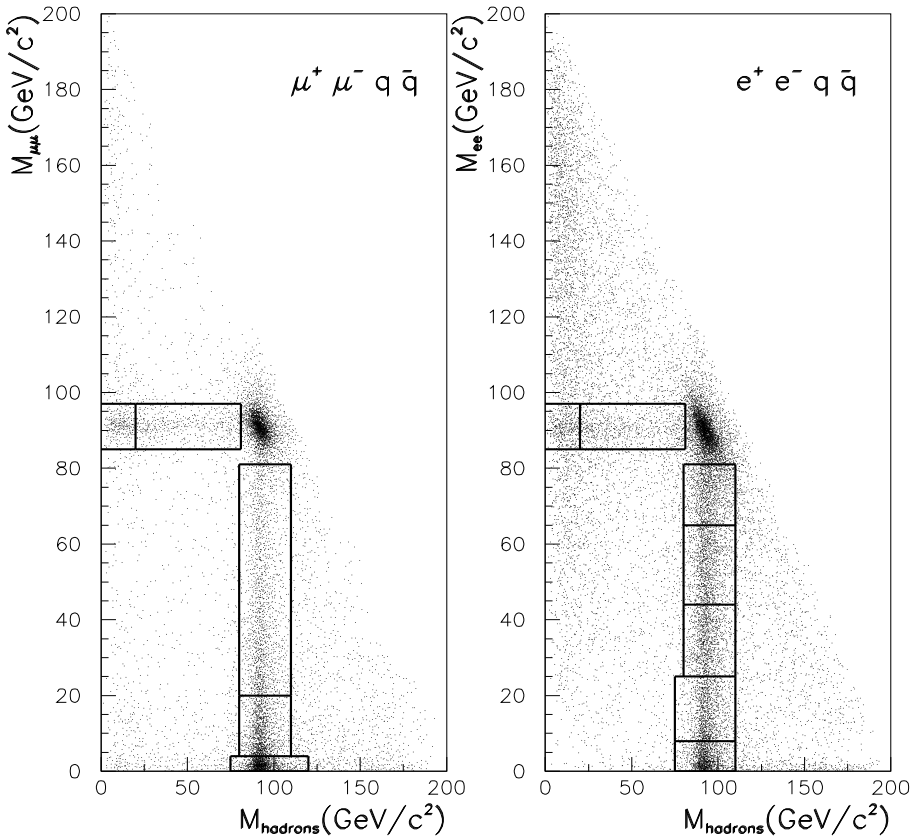

Figure 4: Predicted Standard Model distributions of events in the ($M_{\mu^+\mu^-}$, $M_{q\bar{q}}$) plane and in the ($M_{e^+e^-}$, $M_{q\bar{q}}$) plane, showing the bins used in the fits to the coupling parameters using data from the $Z\gamma^*$ final state.

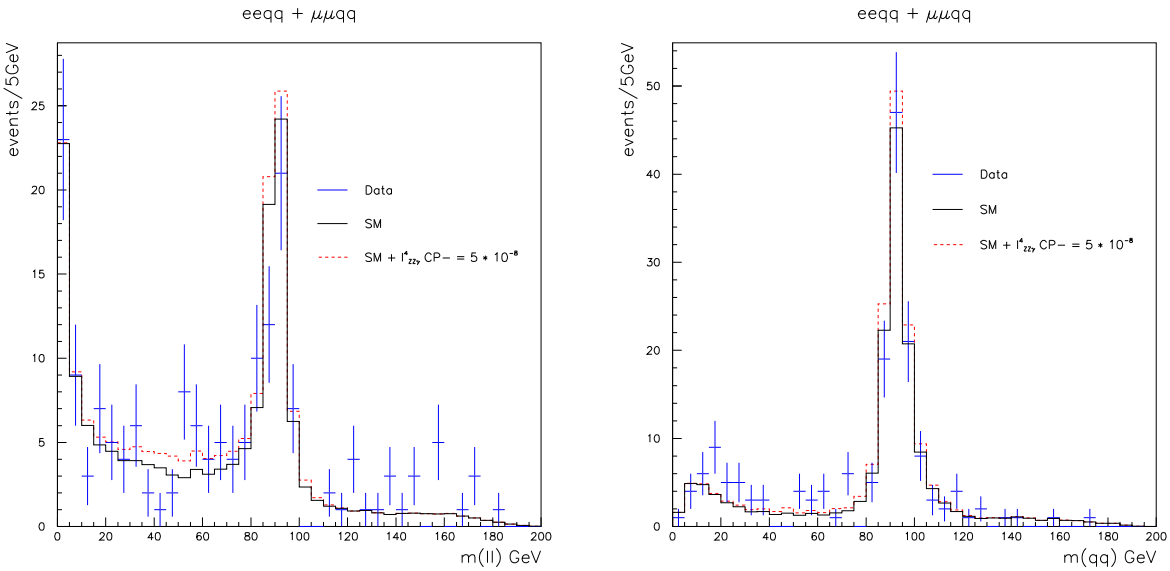

Figure 5: Distributions of $M_{l^+l^-}$ ($l \equiv e, \mu$) and of $M_{q\bar{q}}$, for data selected in the $q\bar{q}\mu^+\mu^-$ and $q\bar{q}e^+e^-$ channels. The experimental data points are shown by crosses, the shaded histograms show the predictions of the Standard Model for signal and background, and the outlined histograms the expectations for a non-standard scenario with a contribution $\tilde{\ell}_4^{ZZ\gamma} m_Z^4 = 3.4$. The parameter $\tilde{\ell}_4^{ZZ\gamma}$, which affects only the $ZZ\gamma^*$ vertex, is defined in table 1.

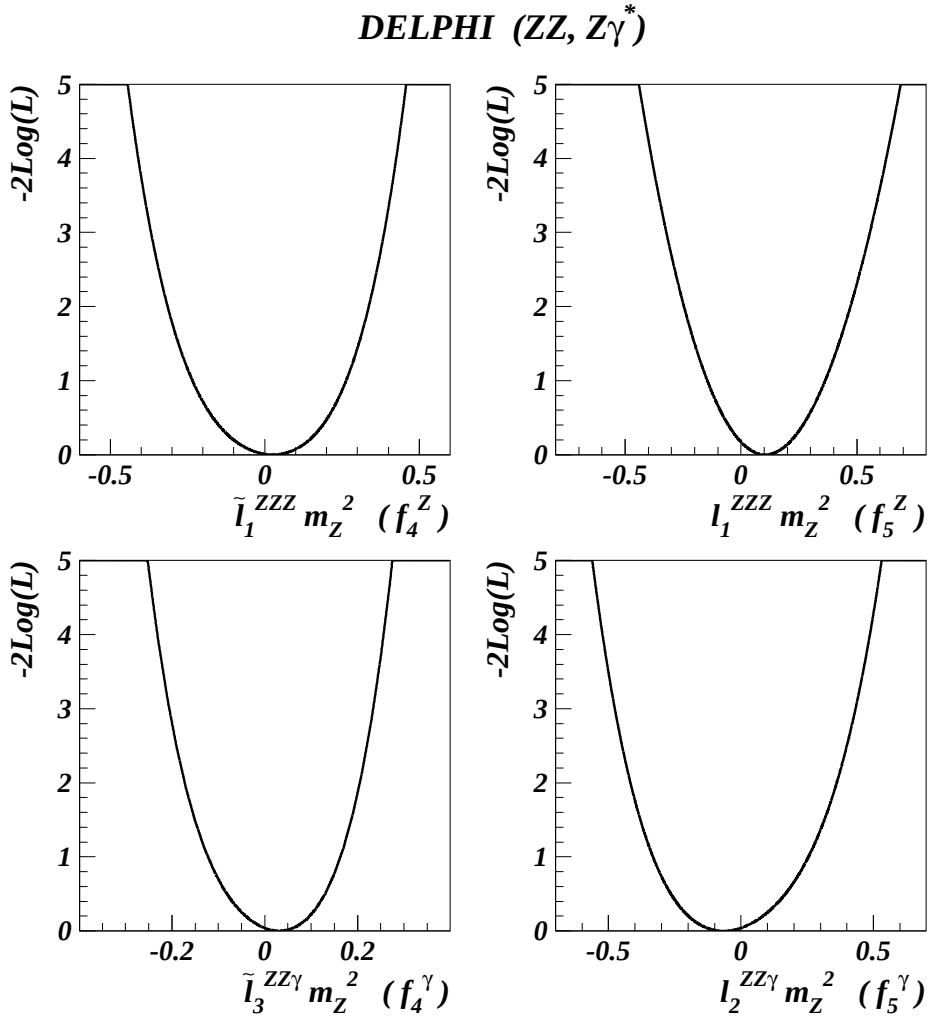

Figure 6: Likelihood distributions for neutral gauge coupling parameters corresponding to Lagrangian operators influencing ZZ and $Z\gamma^*$ production. The parameters are defined in section 1.1; the corresponding on-shell parameters are shown in brackets on the abscissa labels. The distributions include the contributions from both statistical and systematic effects.

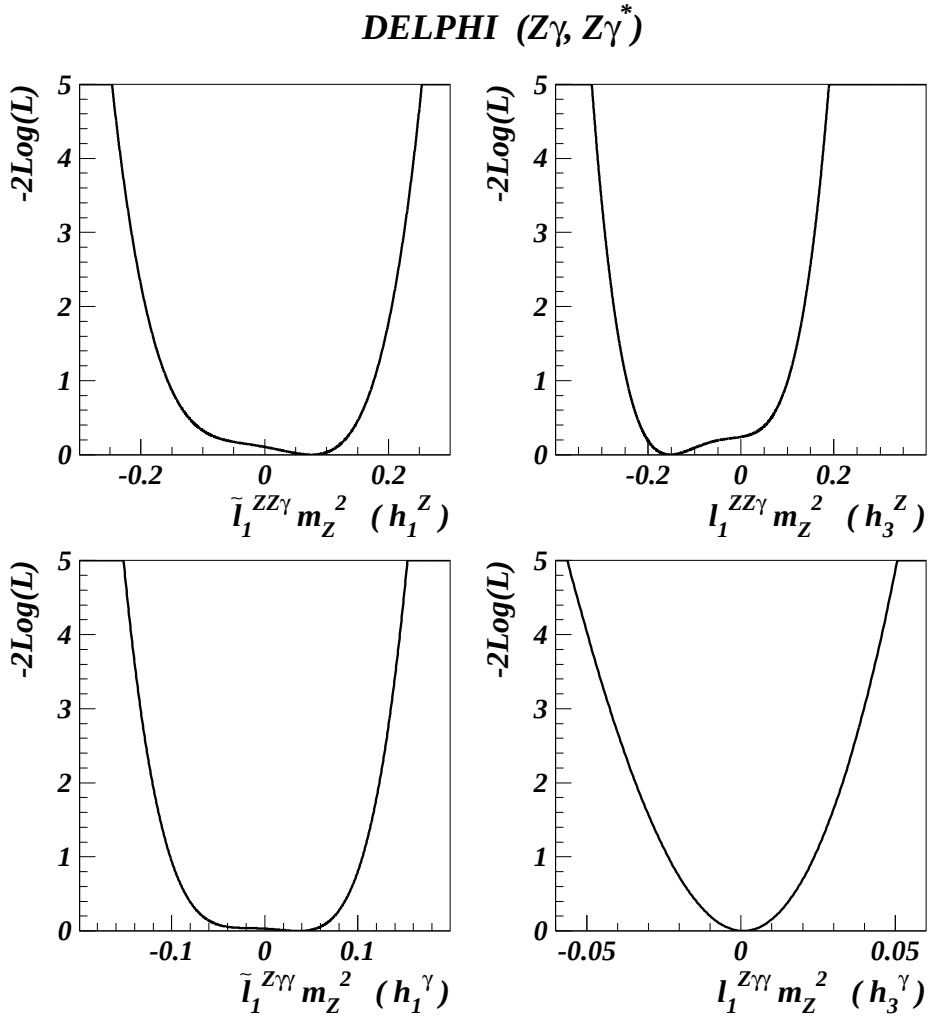

Figure 7: Likelihood distributions for neutral gauge coupling parameters corresponding to Lagrangian operators influencing $Z\gamma$ and $Z\gamma^*$ production. The parameters are defined in section 1.1; the corresponding on-shell parameters are shown in brackets on the abscissa labels. The distributions include the contributions from both statistical and systematic effects.

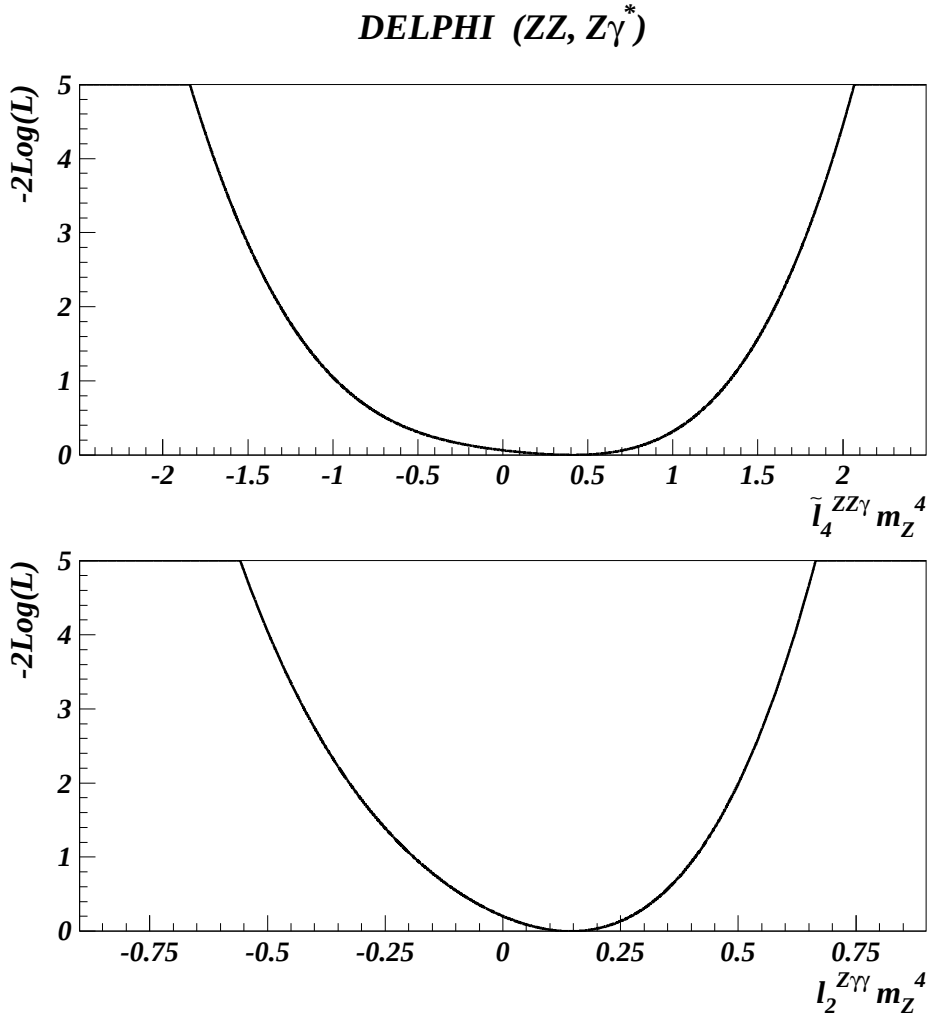

Figure 8: Likelihood distributions for neutral gauge coupling parameters corresponding to Lagrangian operators affecting only the $V^0 Z\gamma^*$ vertices. The parameters are defined in section 1.1. The distributions include the contributions from both statistical and systematic effects.

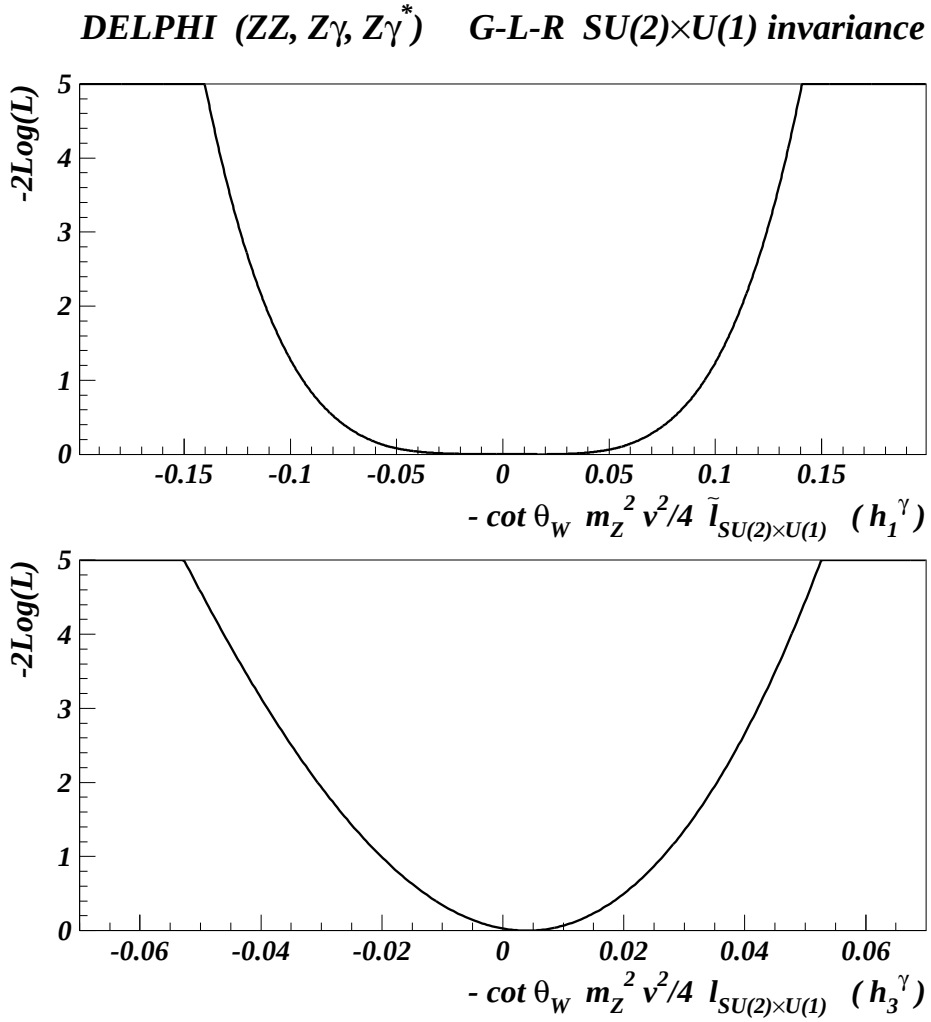

Figure 9: Likelihood distributions for neutral gauge coupling parameters corresponding to $SU(2) \times U(1)$-conserving Lagrangian operators satisfying the Gounaris-Layssac-Renard (G-L-R) constraints. The parameters are defined in section 1.1. The distributions include the contributions from both statistical and systematic effects.

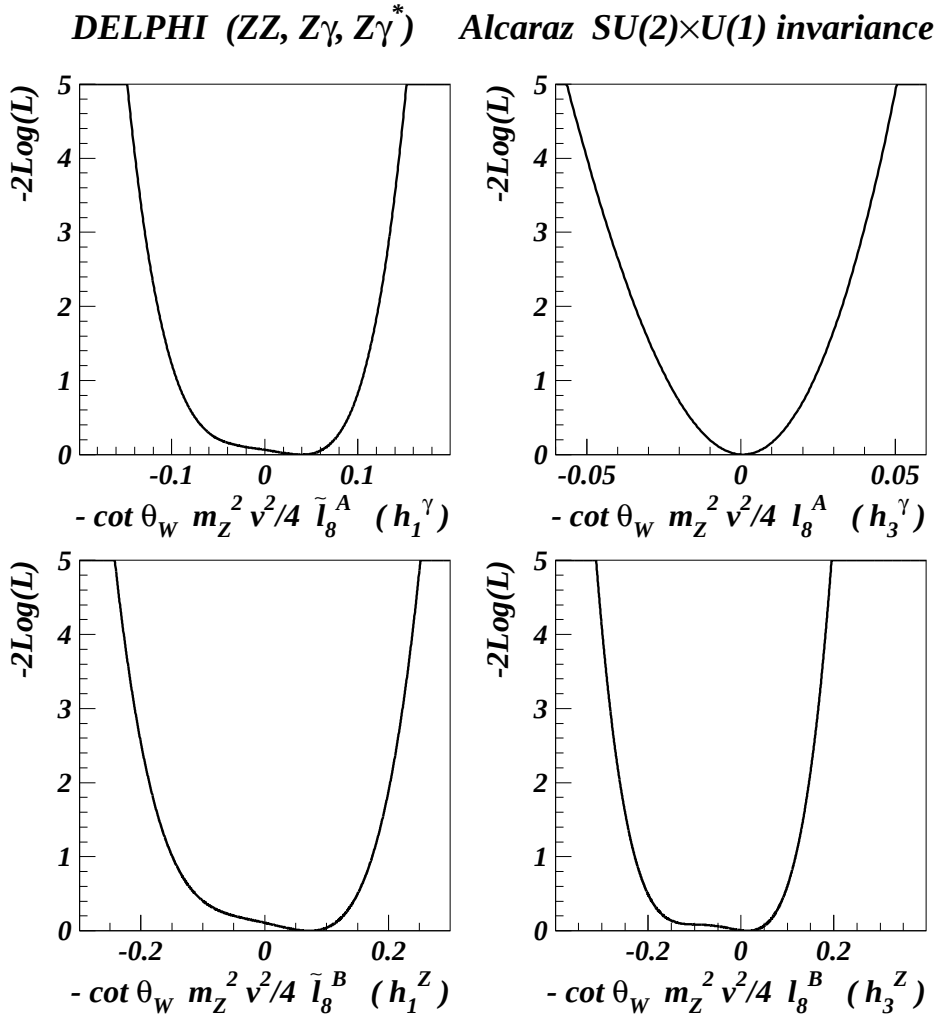

Figure 10: Likelihood distributions for neutral gauge coupling parameters corresponding to $SU(2) \times U(1)$-conserving Lagrangian operators satisfying the Alcaraz constraints. The parameters are defined in section 1.1.